J. of Supercritical Fluids 57 (2011) 87–94

Contents lists available at ScienceDirect

The Journal of Supercritical Fluids

journal homepage: www.elsevier.com/locate/supflu

Two-step micro cellular foaming of amorphous polymers in supercritical CO_2

Jose Antonio Reglero Ruiz[a,*], Jean Marc-Tallon[b], Matthieu Pedros[b], Michel Dumon[a]

[a] Laboratoire de Chimie de Polymères Organiques (LCPO-CNRS UMR 5629), IPB, 16 Avenue Pey-Berland, Université de Bordeaux, 33607 Pessac Cedex, France
[b] Institute Universitaire de Technologie (IUT), Dépt Sciences et Génie des Materiaux, Université Bordeaux 1, 33175 Gradignan, France

ARTICLE INFO

Article history:
Received 5 October 2010
Received in revised form 25 January 2011
Accepted 28 January 2011

Keywords:
Microcellular foaming
Amorphous polymers
Additives
Supercritical carbon dioxide
Nanostructured

ABSTRACT

Microcellular foaming of amorphous rigid polymers, polymethylmethacrylate (PMMA) and polystyrene (PS) was studied in supercritical CO_2 ($ScCO_2$) in the presence of several types of additives, such as triblock (styrene-co-butadiene-co-methylmethacrylate, SBM and methylmethacrylate-co-butylacrylate-co-methylmethacrylate, MAM) terpolymers. This work is focused in the two-step foaming process, in which the sample is previously saturated under $ScCO_2$ being expanded in a second step out of the CO_2 vessel (e.g. in a hot oil bath) where foaming is initiated by the change of temperature near or above the glass transition temperature of the glass/polymer glassy system. Samples were saturated under high pressures of CO_2 (300 bar), at room temperature, for 16 h, followed by a quenching at a high depressurization rate (150 bar/min). In the last step, foaming was carried out at different temperatures (from 80 °C to 140 °C) and different foaming times (from 10 s to 120 s). It was found that cellular structures were controlled selecting either the additive type or the foaming conditions. Cell sizes are ranging from 0.3 μm to 300 μm, and densities from 0.50 g/cm^3 to 1 g/cm^3 depending on the polymers considered.

1. Introduction

Environment-friendly techniques can be used to prepare microcellular foams using supercritical fluids as foaming agents. They have many advantageous properties, which enable their use as foaming agents, such as a tuneable solvent power, the plasticization of glassy polymers (as a consequence of glass transition temperature depression) and enhanced diffusion rates [1,2]. Especially, the use of CO_2 has increased greatly in the last years due to the low critical conditions of CO_2 (31.1 °C and 71 bar) [3,4]. The microcellular foaming process using supercritical CO_2 ($ScCO_2$) allows an easy and complete separation from the polymer, without a vapour–liquid transition during the expansion. There are two main batch routes to produce microcellular foam polymers using $ScCO_2$, namely a one step process (continuous) and two step process (non-continuous). In both processes, the objective is the production of controlled, calibrated foams in the micrometer or submicrometer range, i.e. microfoams or ultramicrocellular polymers.

In the one-step process, the polymer is saturated with CO_2 at a moderate temperatures and high pressures (assuring the supercritical conditions of the gas), followed by the rapid depressurization to atmospheric pressure. This route has been deeply analysed in numerous works, with excellent results in several amorphous polymers such as polystyrene [5], polymethylmethacrylate [6,7] or fluorinated ethylene–propylene copolymers [8]. The second alternative is based on the saturation of the polymer with CO_2 at room temperature and subsequently removes it by heating to a temperature near the T_g of the glass/polymer system in a temperature bath [9,10].

In both cases, the foaming process takes advantage of the plasticization effect which decreases the intrinsic glass transition temperature of the polymer due to the supercritical fluid solubility. This allows to produce microcellular structures in a very broad temperature range, even below the depressed glass transition temperature of the polymer, leading to a solid-state microcellular foaming process [11].

One of the key processes to control the cellular structure is the nucleation and growth of gas cells dispersed throughout the polymer. The resulting structure depends on a balance between several mechanisms, such as diffusion of CO_2 in the polymer, the solubility and the plasticization effect, which depends intrinsically of the polymer and the saturation conditions [12].

In our study, an investigation of the two-step foaming process is carried out. In this process, the polymer is saturated with $ScCO_2$ at high pressures and room temperature. Next, the polymer/gas mixture is quenched into a glassy supersaturated state by reducing the pressure to atmospheric pressure. Finally, in the second step, after removing rapidly the sample from the CO_2 vessel, polymer is foamed by heating to a temperature above or near the depressed glass transition temperature, leading to nucleation and cell growth. Foaming temperature and foaming time are the main parameters to control the cellular structure of the final product leading to macro or micro cellular polymers [13].

* Corresponding author. Tel.: +33 686 125 035.
E-mail address: jareglero@gmail.com (J.A.R. Ruiz).

0896-8446/$ – see front matter © 2011 Elsevier B.V. All rights reserved.
doi:10.1016/j.supflu.2011.01.011

The cell size (expressed by an average diameter ϕ, μm), the cell density (N_C expressed by the number of cells/cm^3) and the foam density (ρ_f, g/cm^3) will be estimated for all the experiments performed, analysing the influence of different additives and processing conditions in the variables exposed previously (diffusion, affinity to CO_2 and viscoelastic behaviour plasticization effect), and consequently in the foaming behaviour.

2. Experimental

2.1. Materials

(a) Homo polymers

Two main neat homopolymers were used.

(1) *High impact transparent polymethylmethacrylate* (*PMMA*) was kindly supplied by Altuglas Company-Arkema (France) in the form of pellets. Experimental details about blending and production of the polymer can be found elsewhere [14,15].

(2) *High molecular weight transparent polystyrene* (*PS Crystal*) was kindly supplied by Total Petrochemicals Company (France), in the form of pellets.

(b) Copolymers and blends

Two neat block copolymers were used as neat materials or as additives in blends with the previous polymers (PS, PMMA). All of them were kindly supplied by Arkema Company (France), in the form of pellets, and used as received.

(1) One triblock styrene–butadiene–methylmethacrylate terpolymer (polystyrene-block-polybutadiene-block-polymethylmethacrylate named SBM) was selected. Composition of the triblock copolymer was as follows: 52 wt% stryrene–30 wt% butadiene–18 wt% methylmethacrylate with a PS block of molar mass equal to 30,000 g/mol.

(2) One triblock methylmethacrylate–butylacrylate–methylmethacrylate terpolymer (poly methylmethacrylate-block-polybutylacrylate-block-polymethylmethacrylate named MAM) with 35 wt% methacrylate–30 wt% butylacrylate–35 wt% methacrylate, with a PMMA block of molar mass equal to 90,000 g/mol.

Two different blends were produced in order to analyse the effect of the additives in the foaming behaviour. First, a PS + SBM blend, with 90 wt% polystyrene–10 wt% SBM). Second, a PMMA + MAM blend, with 90 wt% PMMA–10 wt% MAM. In both cases, blending and extrusion was carried out, and final materials were obtained in the form of transparent pellets.

Table 1 shows the physical properties of the materials employed. Glass transition temperature (T_{g0}) was measured in a DSCQ100 equipment, using a heating cycle from −50 °C to 200 °C at 5 °C/min). Average molar masses (M_w) were determined by size exclusion chromatography in a PL-GPC50Plus device using THF (tetrahydrofuran) as a solvent with a concentration of 3 mg/ml with UV detection at 254 nm. The T_g detected, those mentioned in Table 1, do not necessarily correspond to the T_g of each blocks of the copolymer, because the low values of the T_g in the soft blocks could not be measured in our conditions. Thus, the T_g values are mentioned as detected by DSC.

2.2. Sample preparation

Blends (PS + SBM or PMMA + MAM) were produced as follows: materials were dried in vacuum (680 mm Hg), at 80 °C for 4 h before processing. Mixing and extrusion were carried out using a Scamex CE02 extruder, with a temperature profile from 165 °C to 225 °C, at a screw velocity of 60 rpm.

In a second step, pellets were injected into sheets (50 mm × 15 mm) with 3 mm thickness, using a small scale injection moulding machine developed by DSM Xplore. The working temperature was fixed at 240 °C, whereas mould temperature was 60 °C. The injection pressure was fixed at 12 bar. Samples obtained showed a good surface appearance as well as a good injection behaviour, with no presence of air bubbles inside the sheet. In the case of PMMA + MAM blend, a nanostructured polymer showing wormlike micelles corresponds to the butylacrylate block of MAM triblock, whereas in the case of PS + SBM the micelles are the butadiene block of SBM terpolymer. Moreover, in the PS + SBM blend, the isolated micelles are large enough to scatter light, and the modified polymer is not perfectly transparent, and samples were slightly opaque. On the contrary, in the PMMA + MAM blend the MAM terpolymer is nanostructurated at scales below 100 nm, showing transparent samples, indicating a soluble additive leading into a nanostructured copolymer, as seen in Fig. 1.

2.3. $ScCO_2$ foaming

Microcellular foaming experiments were carried out in a high pressure reactor provided by TOP Industry (France), with a capacity of 300 cm^3 and capable of operating at maximum temperature of 250 °C and maximum pressure of 400 bar. The reactor is equipped with an accurate pressure pump controller provided by Teledyne ISCO, and controlled automatically to keep the temperature and pressure at the desired values. The CO_2 vessel temperature and pressure were monitored in the course of the process.

Several series of experiments were performed in a two-step batch process. In all the experiments, samples were saturated under 300 bar of $ScCO_2$ for 16 h at RT. This time assures the equilibrium dissolution of the gas into the polymer, as seen in the first part of this study. In addition, it is well known that saturation increases at low temperatures, and that is the reason of choosing RT as a saturation temperature. After this process, supersaturated state was quenched by a high depressurization rate down to atmospheric pressure (150 bar/min) without foaming and samples were removed from the vessel. In the foaming process, two main routes were employed. First, the foaming temperature in the hot oil bath was fixed at 100 °C, with foaming times of 10 s, 30 s, 60 s and 120 s.

Table 1
Physical properties of the materials employed.

Material	Glass transition (°C)	Molecular weight (g/mol)	Bulk density (g/cm^3)
PS	103	140,000	1.05
PMMA	111	70,000	1.17
PS + SBM	98	30,000	1.01
PMMA + MAM	109	80,000	1.02
MAM	49 and 95	98,000	1.08
SBM	53 and 109	30,000	1.01

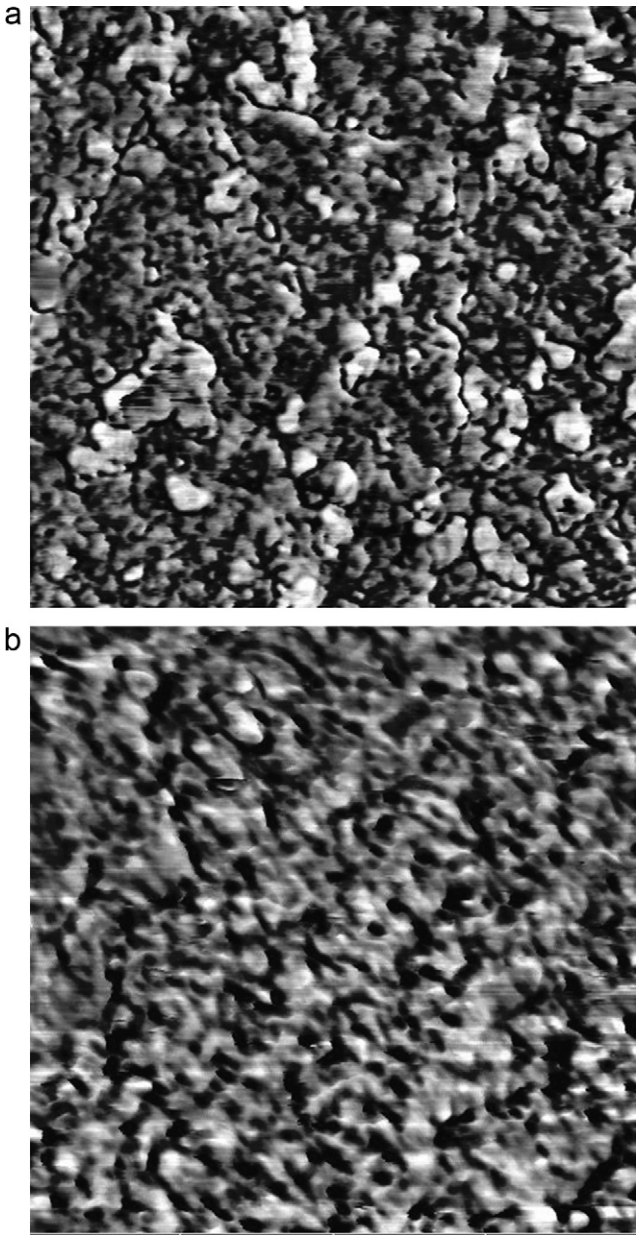

Fig. 1. AFM images of the two blends produced (phase signal data, size 1 μm × 1 μm). (a) PMMA + MAM and (b) PS + SBM.

In the second route, foaming time was fixed at 60 s, with different foaming temperatures of 80 °C, 100 °C, 120 °C and 140 °C. In all the cases, after foaming the cellular structure was frozen in an ice-water bath.

2.4. Foam density

Foam density ρ_f was determined by water-displacement method, based on Archimedes principle. Densities were calculated by measuring the volume of water displaced by the sample divided into the sample mass [16]. In most of the cases due to the gas diffusion a solid outer skin is formed during the foaming process, which must removed mechanically by machining in order to measure only the density of the cellular structure (due to the closed cell structure of the foam samples, there was not uptake of water by the samples during measurements). At least three measurements were carried out for each sample produced.

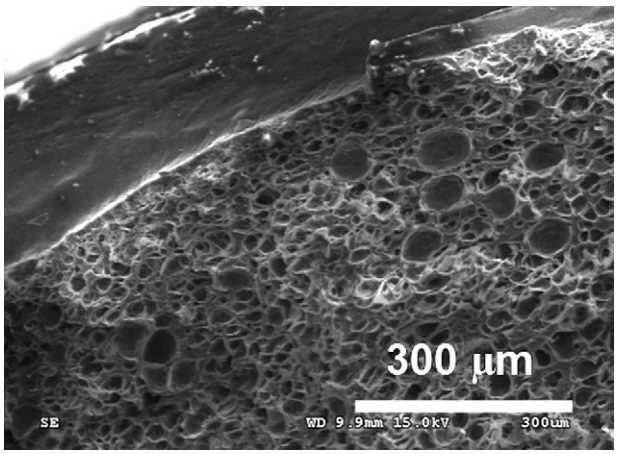

Fig. 2. SEM micrograph of the solid outer skin presented in the samples.

2.5. SEM observations

Average cell size was measured by means of scanning electron microscopy (model HITACHI S-3000N). For the preparation of the samples, foams were frozen in liquid nitrogen and fractured to assure that the microstructure remained intact. For the observations, surfaces were coated with gold using a sputter coater (model EMSCOPE SC 500), in argon atmosphere. The micrographs obtained were analysed to measure cell sizes and assign the presence of a solid outer skin. In Fig. 2 is presented a SEM micrograph of the outer solid skin, with an average thickness between 5% and 10% of the total thickness of the foamed sample.

Cell size ϕ was obtained from direct observation, using a minimum of 100 cells in each calculation, over a minimum of 3 SEM micrographs, taken in the middle region of the foamed samples. An average estimated error of 10% can be considered in the cell size determination. On the other hand, cell density N_C (cells/cm^3) was calculated from the next equation [17]:

$$N_C \cong \left(\frac{nM^2}{A}\right)^{3/2} \quad (1)$$

where n is the number of cells observed in a SEM micrograph, A is the area of the micrograph in cm^2 and M is the magnification factor.

3. Results and discussion

3.1. Sorption of CO_2

One of the key parameters to optimize the microcellular foaming process concerns the absorption kinetics of CO_2 during the saturation process. Experimental data was obtained as follows: samples were removed after the saturation time transferring them to a high precision balance to record the increase in weight due to gas absorption. Several measurements were carried out in the samples for 10 min, observing a small decay in the CO_2 trapped in the sample. During this time, a small quantity of gas escapes from the sample. In our case, for all the samples analysed this decay was inferior to 2%. The final weight of gas presented in the samples is summarized in Table 2 for all the materials at RT after the saturation conditions (300 bar, 16 h).

Results showed in Table 3 presents the quantity of CO_2 uptake w, which quantifies the affinity of CO_2 for the material considered; methacrylate-based polymers and its blends are the most CO_2 philic materials. It is important to remark that after saturation, samples must be foamed in a short period of time, because a great percentage of the gas absorbed is released after a few hours.

Table 2
CO_2 uptake after 16 h saturation in all the materials investigated.

Material	CO_2 uptake (%)
PS	9.2
PMMA	16.4
PS + SBM	12.5
PMMA + MAM	23.3

In our case, a maximum delay of 10 min was set after removing the samples from the vessel and foaming in the hot oil bath. The equilibrium situation in all the gas–polymer systems is completely reached after 16 h of saturation for the given conditions of 300 bar and RT. As already predicted [18], an increase in saturation temperature induces decrease in CO_2 uptake.

Next, predicted glass transition temperatures at RT are needed (T_g), in order to know the relation between the foaming temperature and the plasticization state of the sample after saturation. The predicted values can be calculated from the theoretical prediction of Hwang's model [19] in all the polymer–$ScCO_2$ systems investigated. In this investigation, the relationship between gas absorption and the glass transition temperature in a batch foaming process is analysed, measuring the change in the elasticity modulus induced near the glass transition temperature.

$$T_g = T_{g0}\ \exp[-(M_p)^{-1/3}(\rho_S)^{-1/4}\alpha \cdot w] \quad (2)$$

where α is a material constant determined by both polymer and gas, M_p is the weight average molar mass of the polymer, w is the weight fraction of CO_2 absorbed during the saturation process, T_{g0} is the glass transition temperature of the polymer and ρ_S is the specific density of the polymer.

Theoretical predictions of this model can be calculated considering different α constants. The rest of the experimental parameters employed in the equation can be determined experimentally. Glass transition temperature T_{g0} was measured by means of DSC technique, the specific gravity of the polymer ρ_S is measured using a high precision balance, the molecular weight of the polymer M_p (chosen as M_w) were measured by SEC (see Table 1), and finally the weight fraction of CO_2 absorbed by the polymer w was determined as explained previously (see Section 3.1). Table 3 presents the theoretical predictions of T_g after saturation at RT and 300 bar using $\alpha = 0.7$, the typical value employed in polymer–$ScCO_2$ mixtures at those conditions.

As stated previously, foaming experiments were carried out at temperatures from 80 °C to 140 °C, and the estimation of the glass transition temperature of the gas–polymer system in the supersaturated state is a key parameter to set the polymeric viscoelastic range, which determines the final cellular structure and density of the material.

3.2. Foaming experiments

The two-step foaming process has been analysed, employing two different routes. A common saturation process, under 300 bar of $ScCO_2$ for 16 h at RT was performed in all the samples. After removing the samples from the vessel, a minimum time of 10 min were selected before foaming, to assure that all the CO_2 remains trapped in the sample and all the residual gas has escaped. Then, samples were foamed in a hot oil bath, using two different routes. First, for a fixed foaming temperature of 100 °C different foaming times were investigated. In the second route, for a fixed foaming time of 60 s, different foaming temperatures were analysed. As stated before, cellular structure, defined by the average cell size ϕ, foam density ρ_f and cell density N_C will be affected by two main factors. First, the depression of the glass transition temperature, which was investigated by varying the foaming temperature to produce microcellular materials under different plasticization/vitrification conditions. Secondly, the foaming time will take into account the effect of the diffusion of the gas throughout the polymer and its ability to retain the gas to produce the cellular structure.

3.2.1. Behaviour of homopolymers PMMA and PS

In Fig. 3, we present the cell size evolution in neat PMMA during the foaming process. It is clear that very low cell sizes are obtained in all the cases (below 1 μm), combined with a poor density reduction compared to solid material (density range lies between 0.9 and 1 g/cm^3). It is important to remark that foaming is not possible at very low foaming times, as seen in Fig. 3b.1), where cells have not enough time to grow, and only some nucleated sites are presented. Increasing time leads to the formation of the cellular structure (see Fig. 3b.2), with very low cell size and a regular appearance. On the contrary, varying the foaming temperature has not great influence in the cellular structure, as presented in Fig. 3a.1 and a.2, which indicates that for this particular foaming temperature the enlargement of the plasticization range does not increase the cell size greatly. This effect shows that the CO_2 content is a preponderant effect compared to T_{foam}. When an amorphous polymer is foamed at a sufficiently high temperature (in the rubbery zone), and the foaming time allowed is enough, the gas quantity may control the foaming of PMMA homopolymer (CO_2 philic polymer).

A completely different behaviour is found for the neat PS homopolymer. The cell size evolution is presented in Fig. 4. First, for a fixed foaming temperature of 100 °C, only foaming occurs when using times above 60 s (see Fig. 4b.1 and b.2). Saturation temperature and foaming temperature play a similar role in both processes. On the other hand, for a fixed foaming time of 60 s, foaming is possible all over the temperature range, increasing cell sizes at the same time, from 5 μm to 20 μm, as seen in Fig. 4a.1 and a.2. In this case, although the plasticization is similar as in PMMA (the depressed T_g values are similar as showed in Table 3), higher cell sizes, together with a remarkable density reduction, are achieved when foaming neat PS in these conditions. Again, this can be explained due to the different CO_2 affinity between PS and PMMA. Moreover, the capacity of PMMA to retain the CO_2 molecules after the saturation process is much greater than in PS. For this reason, the number of nucleated sites available in PS is lower than in PMMA, which derives in higher cell sizes and lower cell densities. PMMA is kept plasticized more easily than PS. In other words, high temperature plays a role on cell growth in PS whereas it affects poorly the cell growth of PMMA.

Table 4 presents the variation of the main parameters which define the microcellular material (average cell size ϕ, cell density N_C and foam density ρ_f) for all the homopolymers analysed. In the

Table 3
Depressed glass transition temperatures for all the polymers analysed (saturation conditions 300 bar, RT, 16 h).

Material	Glass transition (°C)	CO_2 uptake (%)	Depressed glass transition (°C)
PS	103	10.4	45
PMMA	111	12.1	50
PS + SBM	98	16.9	36
PMMA + MAM	109	22.3	41
MAM	95	24.1	39
SBM	96	8.3	32

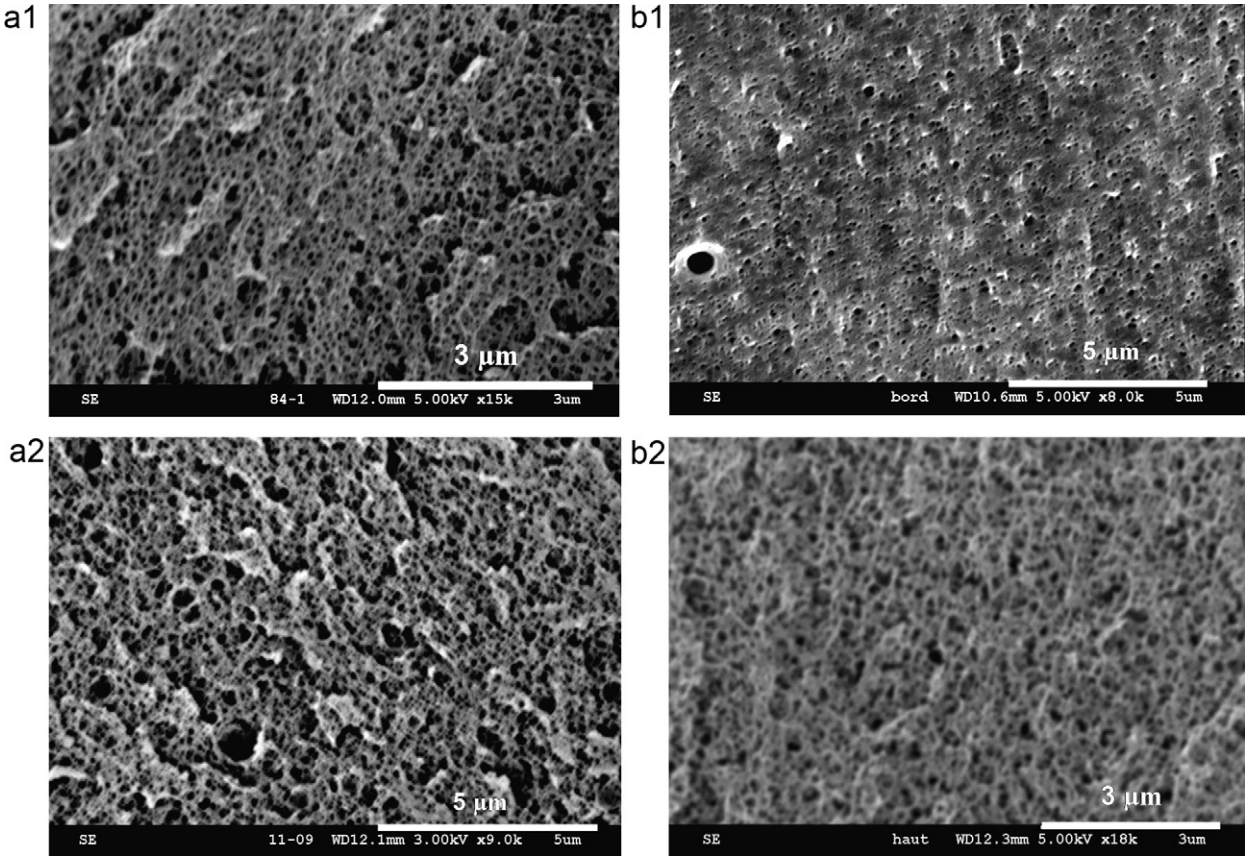

Fig. 3. SEM micrographs showing the cell size evolution in neat PMMA. (a.1 and a.2) At fixed foaming time (60 s) and (b.1 and b.2) At fixed foaming temperature (100 °C).

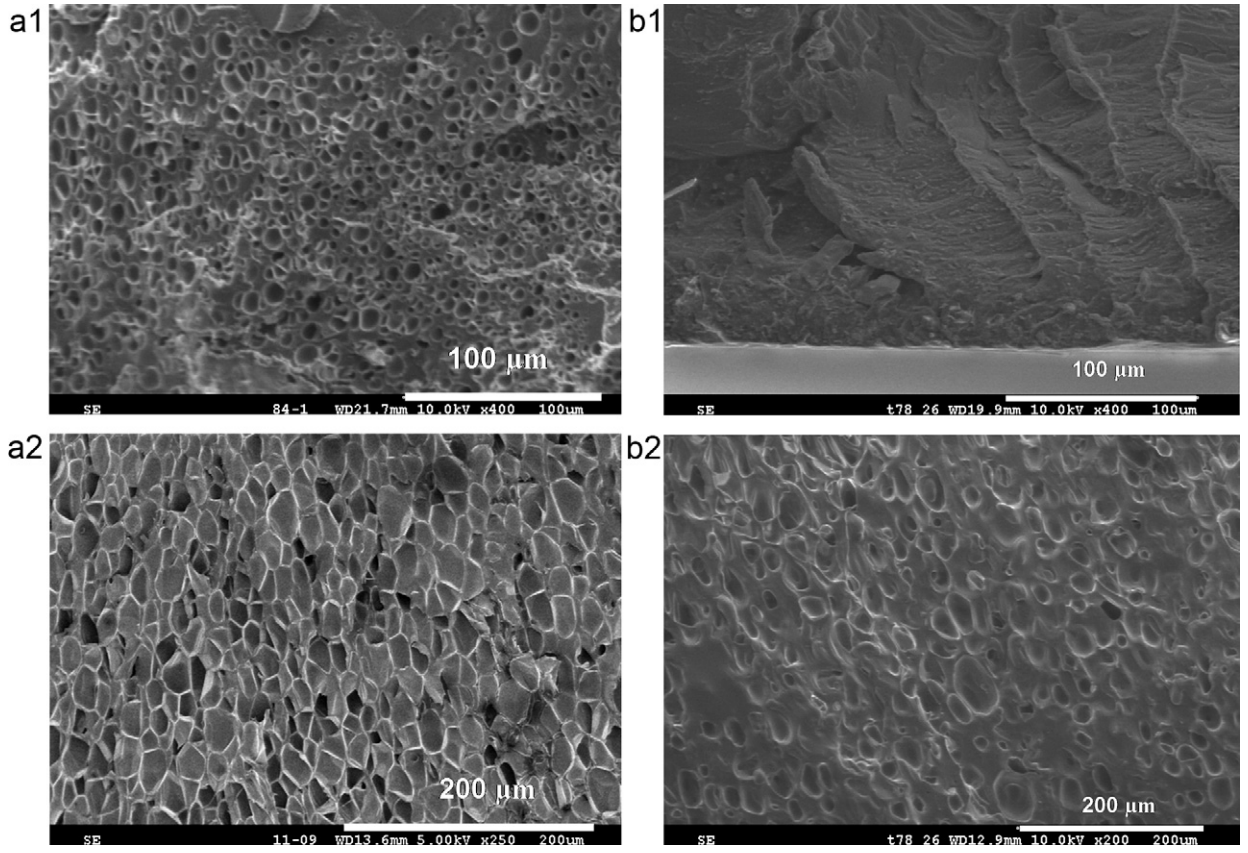

Fig. 4. SEM micrographs showing the cell size evolution in PS foams. (a.1 and a.2) At fixed foaming time (60 s) and (b.1 and b.2) at fixed foaming temperature (100 °C).

Table 4
Main values of ϕ, ρ_f and N_C for the PMMA and PS microcellular foams produced.

	PMMA			PS		
	Cell size (μm)	Foam density (g/cm^3)	Cell density (cells/cm^3)	Cell size (μm)	Foam density (g/cm^3)	Cell density (cells/cm^3)
T_{sat} (°C)						
80	0.3	1.05	7.25×10^{15}	5	1.03	1.82×10^{15}
100	0.35	1.03	5.33×10^{15}	7	0.97	9.51×10^{14}
120	0.4	0.95	4.84×10^{15}	12	0.93	5.37×10^{14}
140	0.5	0.87	3.91×10^{15}	20	0.89	4.57×10^{14}
T_{foam} (s)						
10	NF	NF	NF	NF	1.03	6.66×10^{15}
30	NF	NF	NF	NF	0.91	5.82×10^{14}
60	0.4	10	10	10	0.86	6.29×10^{14}
120	0.5	20	20	20	0.85	5.22×10^{14}

cases in which a foamed material cannot be obtained, a notation NF (not foamed) is included.

As a conclusion, for neat amorphous homopolymers, at comparable depressed glass transition temperatures ($\Delta T_g \approx 60$ °C), a two-step foaming process is very dependent on the CO_2 content introduced in the polymer and the capacity of the polymer to retain CO_2 during foaming. The influence of foaming time is clarified while the influence of foaming temperatures affects only poorly to the CO_2 philic polymers. The time range while growth is allowed and subsequent vitrification (due to T_g crossing) varies between polymers under consideration.

3.2.2. *Behaviour of blends/role of CO_2 philic or nano structured additives in PS or PMMA*

In the last part of the study, we will focus on the analysis of the foaming behaviour of the blends fabricated. As a starting point, we consider the dispersion of the block copolymers as additives in the homopolymers and the improvement in the CO_2 absorption respect to neat homopolymer. For the PS + SBM (90/10 wt%), the SBM copolymer was dispersed at a nanometer level and enhances the CO_2 initial absorption, from 10.4% to 16.9% as seen in Table 3. In the case of PMMA + MAM (90/10 wt%) blend, the MAM was also completely embedded in the matrix resulting into a nanostructured polymer matrix, with a remarkable improvement of the CO_2 absorption (from 12.1% to 22.3%). Fig. 5 presents the SEM micrographs of the PS + SBM blend microcellular foams produced under different foaming conditions, both varying the foaming temperature (Fig. 5a) and varying the foaming time (Fig. 5b).

Results shown in Fig. 5 indicate that PS + SBM can only be foamed at high temperatures (above 100 °C) to produce a cellular structure. The problem of foaming at temperatures above the T_g of neat homopolymer is that the material may flow and it cannot retain its geometric shape in spite of foaming. As it can be seen in Figs. 5a.1 and a.2, average cell size increases with foaming temperature, starting at 10 μm at 80 °C and ending with an average cell size of 30 μm for 140 °C. The influence of the foaming time is also remarkable,

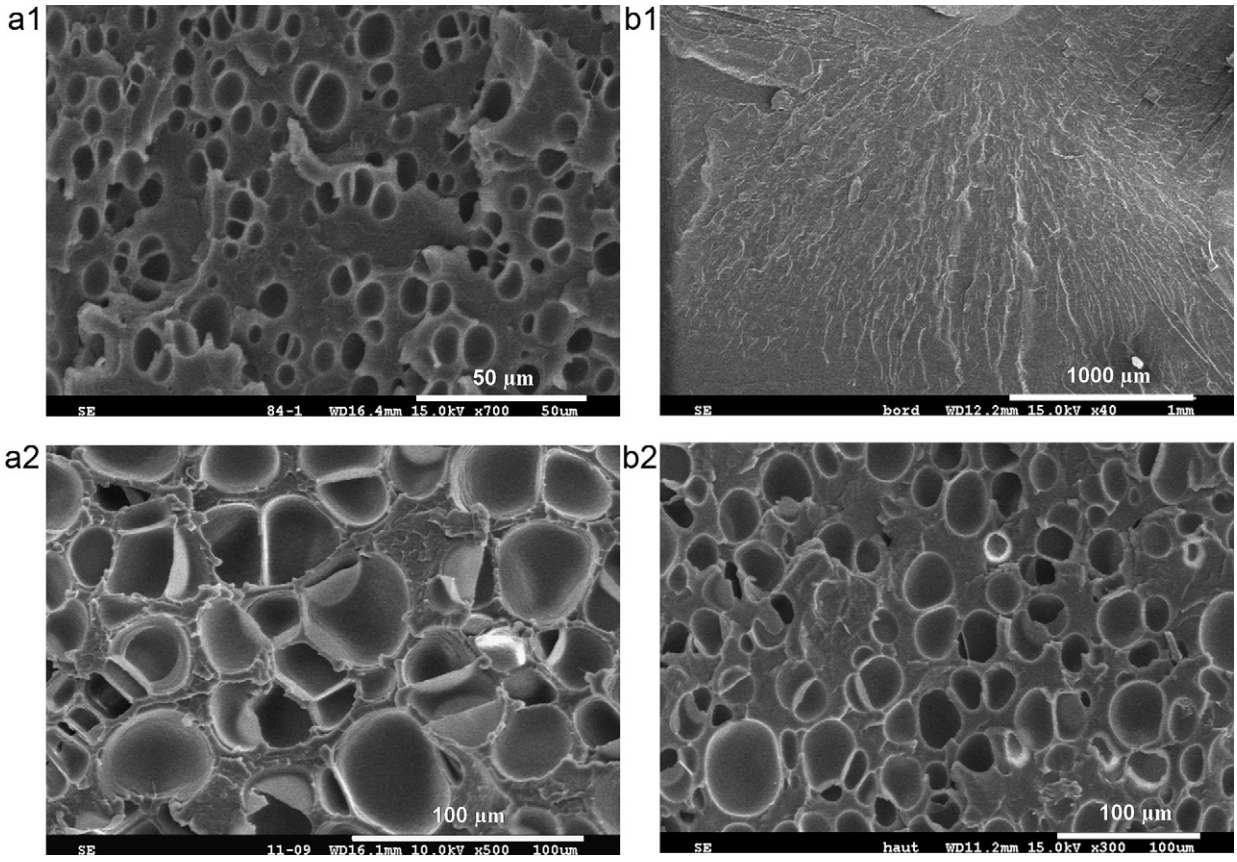

Fig. 5. SEM micrographs showing the cell size evolution in PS + SBM blend. (a.1 and a.2) At fixed foaming time (60 s) and (b.1 and b.2) at fixed foaming temperature (100 °C).

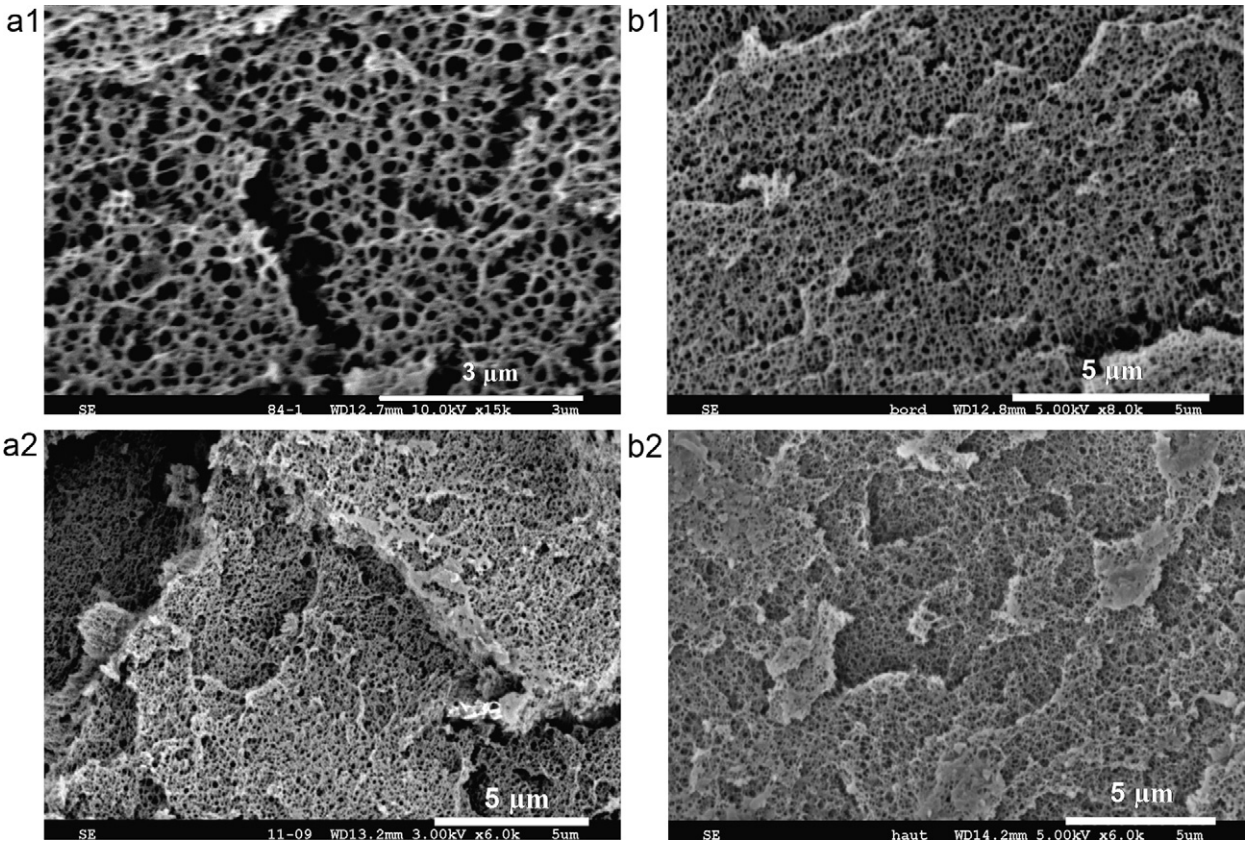

Fig. 6. SEM micrographs showing the cell size evolution in PMMA + MAM blend. (a.1 and a.2) At fixed foaming time (60 s) and (b.1 and b.2) at fixed foaming temperature (100 °C).

Table 5
Main values of ϕ, ρ_f and N_C for the PMMA + MAM and PS + SBM microcellular foams produced.

	PMMA + MAM			PS + SBM		
	Cell size (μm)	Foam density (g/cm^3)	Cell density (cells/cm^3)	Cell size (μm)	Foam density (g/cm^3)	Cell density (cells/cm^3)
T_{sat} (°C)						
80	0.2	0.81	7.34×10^{16}	5	1.02	1.95×10^{12}
100	0.3	0.75	2.53×10^{16}	12	0.91	2.45×10^{11}
120	0.5	0.71	6.02×10^{15}	25	0.90	2.82×10^{10}
140	0.8	0.63	1.72×10^{15}	30	0.82	2.11×10^{10}
T_{foam} (s)						
10	0.4	1.02	3.82×10^{15}	NF	NF	NF
30	0.6	0.95	1.66×10^{15}	NF	NF	NF
60	1	0.92	4.08×10^{14}	NF	NF	NF
120	1.2	0.90	2.55×10^{14}	20	0.98	3.87×10^{10}

and only cellular materials can be produced when using foaming times of 120 s. Comparing this blend to neat PS, to investigate the effect of the additive in the foam formation, a similar behaviour is observed, which indicates a low influence of the SBM additive to improve the main cellular characteristics.

Considering the PMMA + MAM blends, Fig. 6 presents the cellular structure evolution for different foaming conditions.

SEM micrographs reveal a very regular nanocellular structure, with average cell sizes below 1 μm and high cell density values. The cellular structure seems to be unaffected by the processing conditions, keeping the average cell size and the cell density in a very narrow range. It can be only noticed that high foaming temperatures can affect slightly to some cell walls and edges, as seen in Fig. 6a.2. From this, it is evidenced the influence of the MAM additive and the nanostructuration assembly into the PMMA matrix which leads to the formation of nanocellular materials, with a reduction of cell size and an increase of cell density respect to neat PMMA microcellular foams.

An overview of the main foaming characteristics in both blends is presented in Table 5.

4. Conclusions

In this work, the microcellular foaming of several amorphous polymers, polymethylmethacrylate and polystyrene was analysed in a two step process using supercritical CO_2. Several additives were introduced to analyse the effect in the foaming behaviour: triblock (styrene-co-butadiene-co-methylmethacrylate SBM, methylmethacrylate-co-butylacrylate-co-methylmethacrylate MAM) terpolymers. Concerning the CO_2 absorption, experiments were performed at 300 bar and RT for 16 h, showing that methacrylate based polymers presented the highest CO_2 affinity (about 20%) whereas styrene based polymers presented values up to 10%. Considering the plasticization effect, a similar T_g depression was found in all the polymers investigated, with a decrease about 60 °C in the glass transition temperature. To analyse the foaming

behaviour of all the polymers and the influence of the additives employed, two microcellular foaming routes, based in a batch two-step process, were investigated.

In both foaming routes, all samples were saturated under 300 bar of $ScCO_2$ for 16 h at RT, and after removing of the CO_2 vessel were foamed in a hot oil bath.

(a) In the first route, foaming time was fixed at 60 s, and foaming temperatures were varied from 80 °C to 140 °C. For neat homopolymers, it was found that neat PS was able to foam in all the temperature range, with a small influence of the SBM additive in the cellular structure. In the case of neat PMMA a drastic improvement in the cellular structure, reducing the cell size down to nanocellular range, was observed upon addition of the MAM triblock copolymer. The reasons are probably manifolds: nanostructuration of the block copolymer; increase in the global CO_2 uptake and furthermore location of CO_2 in the CO_2-philic rubbery blocks, acting as local CO_2 reservoirs which can be easily plasticized and swollen. Finally, this foaming route revealed as a difficult process to obtain homogeneous cellular structures in all the neat copolymers analysed.
(b) In the second foaming route, foaming temperature was fixed at 100 °C, varying foaming time between 10 s and 120 s. In the case of the two homopolymers, foaming of neat PS was only achieved using high times (120 s), and the addition of the SBM has not considerable effect. Neat PMMA foaming behaviour was similar as observed in previous route. The effect of the addition of MAM triblock copolymer into the PMMA matrix was remarkable, leading to a very stable and homogeneous nanocellular structure with very low cell sizes.

Acknowledgments

This study is part of the LISTRAC (*Lightening of Structures and Composites*) project and funded by the ANR (*Agence Nationale de la Recherche*) which is gratefully acknowledged.

References

[1] A.I. Cooper, Synthesis and processing of polymers using supercritical carbon dioxide, J. Material Chemistry 10 (2000) 207–234.
[2] I. Tsivintzelis, A.G. Angelopoulou, C. Panayiotou, Foaming of polymers with supercritical CO_2: an experimental and theoretical study, Polymer 48 (2007) 5928–5939.
[3] C. Jiang, J. Pi, Q. Pan, Review of supercritical carbon dioxide assisted polymer processing, Polymeric Materials Science and Engineering 25 (2009) 162–165.
[4] P.G. Jessop, W. Leitner, Chemical Synthesis using Supercritical Fluids, Wiley, VCH, Weinheim, 1999.
[5] K.A. Arora, A.J. Lesser, T.J. McCarthy, Preparation and characterization of microcellular polystyrene foams processed in supercritical carbon dioxide, Polymer Engineering and Science 38 (1998) 707–715.
[6] A.V. Nawaby, Y.P. Handa, X. Liao, Y. Yoshitaka, M. Tomohiro, Polymer–CO_2 systems exhibiting retrograde behaviour and formation of nanofoams, Polymer International 38 (2006) 67–73.
[7] S. Huang, G. Wu, S. Chen, Preparation of microcellular cross-linked polyethylene foams by a radiation and supercritical carbon dioxide approach, J. Supercritical Fluids 40 (2007) 323–329.
[8] L. Zirkel, M. Jakob, H. Münstedt, Foaming of thin films of a fluorinated ethylene propylene copolymer using supercritical carbon dioxide, J. Supercritical Fluids 49 (2009) 103–110.
[9] Y. Ito, M. Yamashita, M. Okamoto, Foam processing and cellular structure of polycarbonate-based nanocomposites, Macromolecular Materials and Engineering 291 (2006) 773–783.
[10] X. Han, J. Shen, H. Huang, D.L. Tomasko, L.J. Lee, Effect of block copolymer coated nanoclay on polystyrene foams under supercritical carbon dioxide, Polymer Engineering and Science 47 (2007) 103–111.
[11] C. Barlow, V. Kumar, Impact strength of high density solid-state microcellular polycarbonate foams, J. Engineering Materials and Technology 123 (2001) 229–234.
[12] B. Krause, R. Mettinkhof, N.F.A. van der Vegt, M. Wessling, Bicontinuous nanoporous polymers by carbon dioxide foaming, Macromolecules 34 (2001) 874–884.
[13] R. Sumarno, G.S. Bernardus, A.S. Ismail, P.A. Putu Teta, Chemical reactivity and material processing in supercritical fluids, in: Proceeding of the Eighth Meeting on Supercritical Fluids, 2002, pp. 144–152.
[14] L. Lalande, C.J.G. Plummer, J. Anders, E. Manson, P. Gerard, The influence of matrix modification on fracture mechanisms in rubber toughened polymethylmethacrylate, Polymer 47 (2001) 2389–2401.
[15] C. Dire, B. Charleux, S. Magnet, L. Couvreur, Living character of polymer chains prepared via nitroxide-mediated controlled free-radical polymerization of methyl methacrylate in the presence of a small amount of styrene at low temperature, Macromolecules 40 (2007) 1897–1903.
[16] J.A. Reglero Ruiz, P. Viot, M. Dumon, Foaming behaviour and compressive properties of microcellular nanostructured polystyrene, Cellular Polymers 28 (6) (2009) 363–385.
[17] V. Kumar, N.P. Suh, A process for making microcellular thermoplastic parts, Polymer Engineering and Science 30 (1990) 1323–1329.
[18] Y.-T. Shieng, K.-H. Liu, Solubility of CO_2 in glassy PMMA and PS over a wide pressure range: the effect of carbonyl groups, J. Polymer Research 9 (2002) 107–113.
[19] Y.D. Hwang, S.W. Cha, The relationship between gas absorption and the glass transition temperature in a batch microcellular foaming process, Polymer Testing 21 (2001) 269.